Journal of Quantitative Spectroscopy & Radiative Transfer 129 (2013) 254–262

Contents lists available at ScienceDirect

Journal of Quantitative Spectroscopy & Radiative Transfer

journal homepage: www.elsevier.com/locate/jqsrt

Laser-induced plasma characterization using line profile analysis of chromium neutral atom and ion transitions

Diego M. Díaz Pace *

Instituto de Física 'Arroyo Seco', Campus Universitario, Fac. de Cs. Exactas, UNICEN, Pinto 399, B7000GHG Tandil, Buenos Aires, Argentina

ARTICLE INFO

Article history:
Received 3 May 2013
Received in revised form
24 June 2013
Accepted 25 June 2013
Available online 9 July 2013

Keywords:
LIBS
Self-absorption
Inhomogeneous plasma
Plasma characterization

ABSTRACT

In this paper, line profile analysis of several Cr transitions was carried out for characterization of a laser-induced plasma. The plasma was generated on a metallic alloy (nominal Cr concentration 29.7%) in air at atmospheric pressure by using an infrared Nd:YAG laser. The emission intensities of 24 Cr I lines and 25 Cr II lines were measured spatially integrated along the line-of-sight with good resolution. Their line profiles were analyzed applying a computational fitting algorithm under a framework of a homogeneous plasma in thermodynamic equilibrium. The effects of self-absorption and spatial inhomogeneity were taken into account. The plasma temperature and the parameters *Nl* (the atom/ion concentration times the length of the plasma along the line-of-sight) were accurately determined, and the electron density was estimated. The results were properly interpreted under the employed approach, demonstrating the important influence of the issues investigated on characterizing the physical state of laser-induced plasmas.

1. Introduction

Laser-induced breakdown spectroscopy (LIBS) is an optical technique based on the spectral measurement of the radiation emitted by a laser-induced plasma (LIP) for chemical analysis of the elemental composition of solid, liquid and gaseous targets [1–3]. The LIP can be characterized through determination of the temperature, the electron density, and the atom/ion number densities of the present species [4]. Plasma characterization is of prime importance to achieve a better insight of the physical processes involved in its dynamic behavior and, thus, improving the applications. A recent review by Hahn et al. [5] summarized the current state-of-the-art on this issue and highlighted the necessity of further research to accomplish the full LIBS potential as analytical method.

A reliable characterization of the LIP is essential to LIBS studies devoted to both basic and applied investigations. For instance, two important LIBS approaches relying on accurate plasma characterization are (i) calibration-free (CF-LIBS) methods, which are aimed at obtaining quantitative results without the need for calibration standards [6], and (ii) the use of LIPs as spectroscopic sources for measurement of atomic parameters such as Stark broadenings [7–10] and transition probabilities [11–15]. In the characterization procedure, the plasma temperature has a crucial relevance because it governs the particle–radiation interaction processes in the plasma [16]. The temperature is generally estimated as the first step and, then, subsequently employed in the calculation of the other physical parameters, i.e., electron, atom and ion densities. Therefore, if an inaccurate value of the temperature is obtained, this will cause even larger uncertainties in the subsequent calculus of other plasma parameters and, finally, in the elemental concentrations.

The most frequently used method to determine the temperature is the Boltzmann plot, which is constructed with the line intensities measured from different transitions from one ionization species, i.e., atoms or ions, with available spectroscopic data. The Boltzmann plot provides the excitation temperature from the single species assuming a spatially

* Tel.: +54 249 4439660x1; fax: +54 249 4439669.
E-mail addresses: ddiaz@exa.unicen.edu.ar, diegodiazpace@hotmail.com

0022-4073/$ - see front matter © 2013 Elsevier Ltd. All rights reserved.
http://dx.doi.org/10.1016/j.jqsrt.2013.06.023

homogeneous optically thin plasma in local thermodynamic equilibrium (LTE). In order to achieve an accurate calculus of the temperature, a large number of different lines having a widespread range of upper level energies should be measured. Even higher accuracy is obtained by including in the same plot, called Saha–Boltzmann plot, lines of both atoms and ions (or any two successive ionization stages) of a given element because the level energy difference results increased by the ionization energy [4]. In this case, the ionization temperature is obtained under the same assumptions as the Boltzmann plot method. For a plasma in LTE, the excitation and ionization temperatures coincide with the electronic temperature corresponding to the Maxwell's distribution of electron velocities [17].

Most LIBS experiments are carried out recording spatially-integrated line intensities from LIPs generated in air atmosphere. This configuration is generally chosen because of its simplicity and versatility, which make feasible many applications [18]. Nevertheless, it is well-known that LIPs are very complex sources of radiation which evolve with time; hence, the description of its physical state based on the measurement of emitted radiation is not straightforward. For a given time of observation, self-absorption of spectral transitions and spatial inhomogeneity of the plume make difficult the characterization of the LIP. They affect the line emission intensities leading to inaccurate results for the plasma parameters. The problem of evaluating and compensating self-absorption of spectral lines has been widely discussed in the literature [19–25]. Models of inhomogeneous plasmas has been also reported [26–31], but these are intrinsically more elaborated and time-consuming, which may reduce their practical applicability.

In addition, from an experimental point of view, there are some issues that should be considered. First, since the plasma properties depend on the experimental parameters, self-absorption and inhomogeneity can be overcome or reduced by a proper choice of measurement conditions and/or selection of adequate emission lines, as shown for instance in Refs. [32,33]. Consequently, after adequate conditions of measurement are matched, those lines showing a plateau (which indicates strong self-absorption) or a self-reversal dip at its top (evidence of a non-uniform distribution of temperature along the direction of observation) are usually discarded. In this way, the characterization is simplified by adopting the approach of an optically thin, homogeneous plasma in LTE. However, depending on the particular experiment and the analyte, optically thin lines could be scarce or hardly detected, i.e. because of a poor signal or spectral interference. On the other hand, recording many emission lines is advisable to achieve an accurate determination of plasma temperature by means of a Boltzmann plot or a Saha–Boltzmann plot. From the reasons mentioned, the measurement of spectral lines affected by some degree of self-absorption as well as inhomogeneity is generally necessary, and almost unavoidable, for an accurate plasma characterization. In this context, it is worth to further investigate how self-absorption and spatial inhomogeneity impact on the determination of the plasma parameters, specially the plasma temperature.

The study of spectral line shapes is of great importance as a diagnostic tool of LIPs because they provide information on physical source conditions [34]. On these steps, the goal of the present work was the analysis of line profiles of several Cr transitions for characterization of a LIP generated on a metallic alloy. In this approach, several lines of Cr I and Cr II with different spectroscopic features were studied applying a simple model of a homogeneous plasma to extract information about plasma features, with special emphasis in a reliable temperature determination. The information of this study will be useful to LIBS experiments in which an accurate plasma characterization is required and also to obtain some insight about the physical processes involved, such as self-absorption and spatial distribution of species in the plume.

2. Theoretical: spectral line emission from a homogeneous plasma in LTE

In this section, the basic equations describing radiation in the case of homogeneous plasma approximation are reminded. The plasma is assumed in LTE and cylinder-symmetrical. The emission and absorption of radiation are described by an emission coefficient ε_λ ($W\,m^{-3}\,sr^{-1}\,nm^{-1}$) and an absorption coefficient $\kappa(\lambda)$ (m^{-1}), respectively. The wavelength-dependent intensity I_λ ($W\,m^{-2}\,sr^{-1}\,nm^{-1}$) of a spectral line emitted along the line-of-sight is given by the solution to the equation of radiation transfer [35]:

$$I_\lambda = C U_\lambda(T)(1-e^{-\tau_\lambda(T)}) \tag{1}$$

where C (a. u.) is a factor that unifies units and depends on the instrumental set-up, U_λ ($W\,m^{-2}\,sr^{-1}\,nm^{-1}$) is the distribution for blackbody radiation, T (K) is the plasma temperature, and τ_λ (dimensionless) is the wavelength-dependant optical thickness of the plasma. For a plasma in LTE, τ_λ can be separated into different contributing factors, similarly to Ref. [36], as

$$\tau_\lambda(T) = \kappa(\lambda)\ \ l = \kappa_e(T)\, N\, l\, P(\lambda) \tag{2}$$

where $\kappa_e(T)$ (m^3) is a coefficient that depends on the atomic parameters of the transition and that can be calculated if the plasma temperature is known. Namely,

$$\kappa_e(T) = \frac{\lambda^4}{8\pi c\, Q(T)} A_{ji}\ \ g_j\ \ e^{-E_i/kT}(1-e^{(E_i-E_j)/kT}) \tag{3}$$

where λ (m) is the line wavelength, A_{ji} (s^{-1}) is the transition probability, g_j (dimensionless) is the degeneracy of the upper energy level, and E_i, E_j (eV) are the energy of the levels. N (m^{-3}) is the density of the emitting species in the plasma, l (m) is the length of the plasma along the line-of-sight, $P(\lambda)$ (m^{-1}) is the normalized line profile, in general described by a Voigt profile, and $Q(T)$ (dimensionless) is the atomic partition function.

The optical thickness τ_λ reaches its maximum value τ_0 at the line center λ_0 and decreases toward the line wings. If self-absorption of radiation within the plasma is negligible, $\tau_0 \ll 1$ and the plasma is said to be optically thin. On the other hand, for the stronger lines (generally the resonant) the radiation emitted has a large probability of

being absorbed, then, $\tau_0 \gg 1$ and the plasma is said to be optically thick.

A correction factor R_λ (adim.) defined as

$$R_\lambda \equiv \frac{I_\lambda^{thin}}{I_\lambda} = \frac{\tau_\lambda}{1-e^{-\tau_\lambda}} \tag{4}$$

can be calculated if the optical thickness τ_λ is known [23,25,37]. The correction factor R_λ can be subsequently applied to the measured profiles to retrieve the optically thin line profiles for the same number density of emitters.

In order to quantify the effect of self-absorption on the emission line intensity, a coefficient *SA* is defined using the ratio of the measured peak intensity ($I(\lambda_0)$) over its value in absence of self-absorption ($I^{thin}(\lambda_0)$), namely

$$SA \equiv 1 - \frac{I(\lambda_0)}{I^{thin}(\lambda_0)} = 1 - \frac{1}{R_0} \tag{5}$$

where R_0 is the particular value of R_λ (Eq. (4)) at the line peak (λ_0). The *SA* coefficient can be expressed as percentage multiplying Eq. (2) by 100. It should be noted that *SA* was defined here slightly different than that in Refs. [19,20], in such a way that $SA=0$ (or 0% absorbed) if the line is optically thin and it increases up to 1 (or 100%) as the line becomes self-absorbed. Both definitions are equivalent.

The optical thickness of spectral lines governs their self-absorption (see Eqs. (5) and (6)). Similarly to the work of Aguilera et al. [36], it is deduced that the abscissa of the point of intersection of the asymptotes of Eq. (1) for low and high values of the optical thickness is $\tau_0=1$. This is the value of the optical thickness at which self-absorption of a spectral line becomes important. For $\tau_0=1$ $SA=35\%$. Hence, lines with $SA \leq 35\%$ suffer a low to moderate self-absorption. On the contrary, lines with $SA > 35\%$ are significantly self-absorbed.

Integrating both sides of Eq. (2) along the line profile,

$$A \equiv \int_{line} \tau_\lambda \, d\lambda = \kappa_e(T) N \, l \tag{6}$$

we obtain

$$N \, l = A/\kappa_e(T) \tag{7}$$

which is the product of the particle density (atoms/ions) (m^{-3}) and the optical length of the plasma (m) along the line-of-sight. The parameter *Nl* (m^{-2}) is relevant to characterize the plasma in addition to the plasma temperature and the electron density [32,33].

3. Experimental

3.1. Experimental set-up

A schematic representation of the experimental set-up is shown in Fig. 1. It is based on a monochromator with good spectral resolution allowing a detailed measurement of line profiles. It has been used previously [25,37], so only a brief description is given here.

The LIPs were generated in air at atmospheric pressure by focusing a Nd:YAG laser (Continuum Surelite II, $\lambda=1064$ nm, 7 ns pulse FWHM, 60 mJ/pulse, repetition rate 4 Hz) at right angles onto a metallic alloy (nominal concentrations: 63.2% Co, 29.7% Cr, 5.5% Mo, and other trace elements < 2.6%), fixed to a rotary holder, using a quartz lens of 10 cm focal length. The light emitted by the plasma from its brightest central region was collected at right angles to the laser beam direction by using a second quartz lens with a focal length of 20 cm and imaged on the

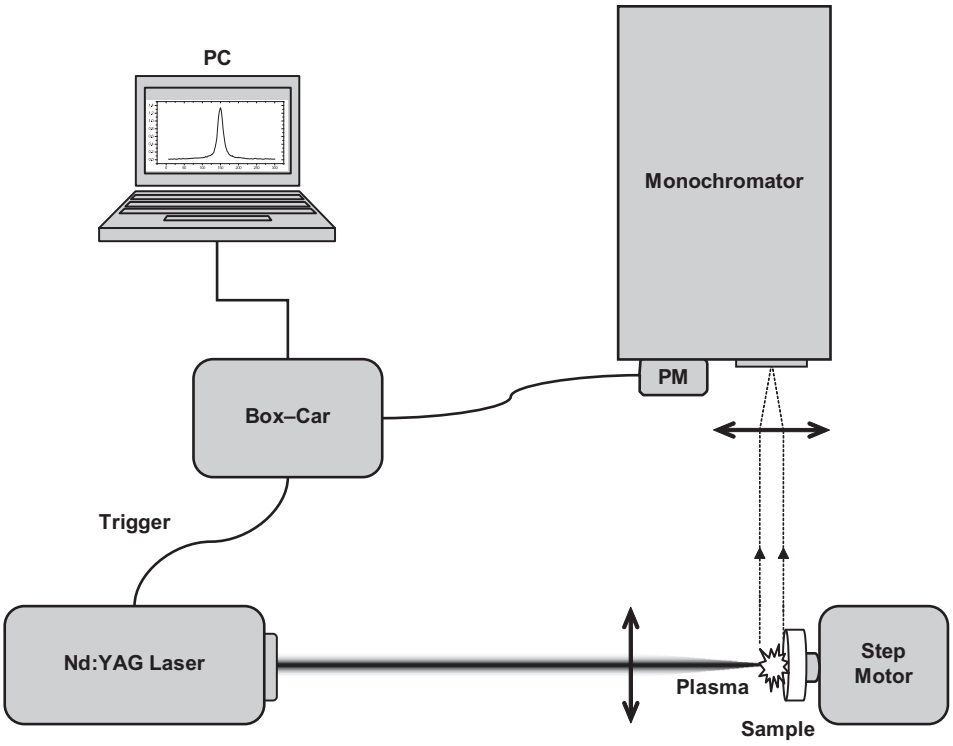

Fig. 1. Experimental set-up.

entrance slit (50 μm-width) of a spectrograph (Jobin Yvon THR 1500, Czerny–Turner configuration, resolution 0.01 nm in double pass at $\lambda = 300$ nm, focal length 1.5 m, grating of 2400 lines/mm). The detector was a photomultiplier (PM) whose signal was time resolved and box-car averaged.

Cr was selected as analyte because it was present in the sample at a relatively high concentration and it has a rich spectrum with an extensive number of transitions. In this way, intense emissions of many Cr I–II lines were measured with a suitable temporal window of 90 ns (Gate width) delayed 4 μs from the laser pulse (delay time). The emission line profiles were scanned moving the diffraction grating of the monochromator controlled by software and synchronized with data acquisition and laser firing. Each experimental point of the emission profile was averaged for 10 laser shots to improve the signal-to-noise ratio (SNR). The instrumental function had an estimated FWHM of 0.0065 nm for the 50 μm-width entrance/exit slits. Line profiles were corrected for the spectral efficiency of the detector and analyzed with a PC employing a self-designed computational algorithm.

3.2. Selection of analytical lines

Several Cr lines with wavelengths in the spectral range 280–450 nm were measured. The following criteria were adopted for selecting the lines:

(i) In typical LIBS experiments, higher ionized species are not present to a significant degree; thus, only transitions from neutral atomic (Cr I) and singly ionized species (Cr II) were considered.
(ii) Emission lines having available atomic data were chosen.
(iii) Lines with different transition probability values $A_{ji} \geq 10^6\ s^{-1}$, and within a broad range of upper level energies were chosen.
(iv) Lines affected from interferences of other elements, with a poor SNR, or exhibiting a self-reversal dip at its top (which is a clear evidence that are strongly absorbed in an inhomogeneous plasma [38]) were discarded.

The selected emission lines were 24 lines of Cr I and 24 lines of Cr II, which are listed in Table 1. The spectroscopic data were taken from the NIST Database [39]. It should be mentioned that the recorded set of lines was not intended to cover the whole Cr spectrum; in fact, other Cr lines could be selected. The employed emission lines included a reasonably large number of lines with different spectroscopic characteristics, which were appropriate for the purpose of the work.

4. Results and discussion

4.1. Analysis of line profiles

The analysis of emission line profiles was carried out employing the method reported in previous works [25,37], which is based in modeling emission line profiles. Basically, a framework of a homogeneous plasma in LTE is applied to extract information about plasma properties from the optical thicknesses of the lines. The optical thickness τ_λ (Eq. (2)) was represented by a pseudo-Voigt function, whose Lorentzian width is dominated by Stark broadening while the Gaussian width is associated to the instrument profile. Self-absorption can be quantified and subsequently compensated to retrieve the optically thin line profiles. In this approach, the intensities of emission of all the Cr I–II lines of Table 1 were computed and matched to their experimental profiles using a fitting algorithm. Two examples of modeling line profiles are shown in Fig. 2.

The results obtained from the analysis of the line profiles are reported in Table 2. The spectroscopic data obtained for each spectral line are the total intensity (I_{tot}), the intensity in

Table 1
Spectral lines of neutral (I) and single ionized (II) atomic lines of Cr analyzed in this work and their spectroscopic parameters (data from [39]).

Species	Wavelength (nm)	A_{ji} (s^{-1})	E_j (eV)	E_i (eV)	g_j	g_i
Cr I	380.48	6.90×10^7	6.28	3.01	9	9
Cr I	391.92	9.20×10^6	4.19	1.03	9	9
Cr I	392.10	5.80×10^6	4.14	0.98	3	5
Cr I	392.86	5.20×10^6	4.16	1.00	5	7
Cr I	394.15	2.80×10^6	4.17	1.03	7	9
Cr I	396.37	1.30×10^8	5.67	2.54	15	13
Cr I	396.97	1.20×10^8	5.67	2.54	13	11
Cr I	398.39	1.05×10^8	5.65	2.54	9	7
Cr I	399.11	1.07×10^8	5.65	2.54	7	5
Cr I	403.91	6.70×10^7	6.92	3.85	15	15
Cr I	406.57	3.50×10^7	7.15	4.10	11	9
Cr I	412.65	6.71×10^6	5.55	2.54	13	13
Cr I	420.45	3.10×10^7	6.93	3.98	11	13
Cr I	426.31	6.40×10^7	6.76	3.85	17	15
Cr I	429.77	4.90×10^7	6.73	3.85	13	11
Cr I	430.05	1.90×10^7	6.32	3.43	7	9
Cr I	433.76	5.48×10^6	3.83	0.97	5	3
Cr I	433.94	6.92×10^6	3.84	0.98	3	1
Cr I	434.45	1.10×10^7	3.86	1.00	9	7
Cr I	435.10	4.18×10^6	3.82	0.97	3	3
Cr I	435.18	1.20×10^7	3.88	1.03	11	9
Cr I	435.96	5.40×10^6	3.83	0.98	5	5
Cr I	437.13	4.10×10^6	3.84	1.00	7	7
Cr I	449.69	3.30×10^6	3.70	0.94	7	5
Cr II	284.32	6.40×10^7	5.88	1.52	10	8
Cr II	285.68	4.30×10^7	6.77	2.43	6	4
Cr II	285.74	2.80×10^7	6.79	2.45	8	6
Cr II	286.09	6.90×10^7	5.81	1.48	4	2
Cr II	286.26	6.30×10^7	5.85	1.52	8	8
Cr II	286.71	1.10×10^8	6.76	2.43	4	4
Cr II	286.76	1.10×10^8	5.80	1.48	2	2
Cr II	287.04	1.30×10^8	6.77	2.45	6	6
Cr II	287.38	8.80×10^7	6.75	2.43	2	4
Cr II	287.84	7.40×10^6	5.85	1.55	8	10
Cr II	288.09	7.90×10^7	6.76	2.45	4	6
Cr II	289.85	1.20×10^8	8.15	3.87	12	10
Cr II	292.18	9.00×10^7	8.11	3.86	10	8
Cr II	293.08	1.10×10^8	7.94	3.71	4	2
Cr II	293.51	1.80×10^8	8.05	3.83	8	6
Cr II	295.34	1.80×10^8	7.91	3.71	2	2
Cr II	296.60	5.40×10^7	8.05	3.87	8	10
Cr II	297.19	2.00×10^8	7.94	3.77	14	14
Cr II	297.97	1.80×10^8	7.92	3.76	12	12
Cr II	298.92	2.20×10^8	7.88	3.75	8	8
Cr II	311.86	1.70×10^8	6.40	3.74	4	2
Cr II	312.04	1.50×10^8	6.41	2.42	6	4
Cr II	312.87	8.10×10^7	6.40	2.43	4	4
Cr II	313.67	6.40×10^7	6.41	4.18	6	6

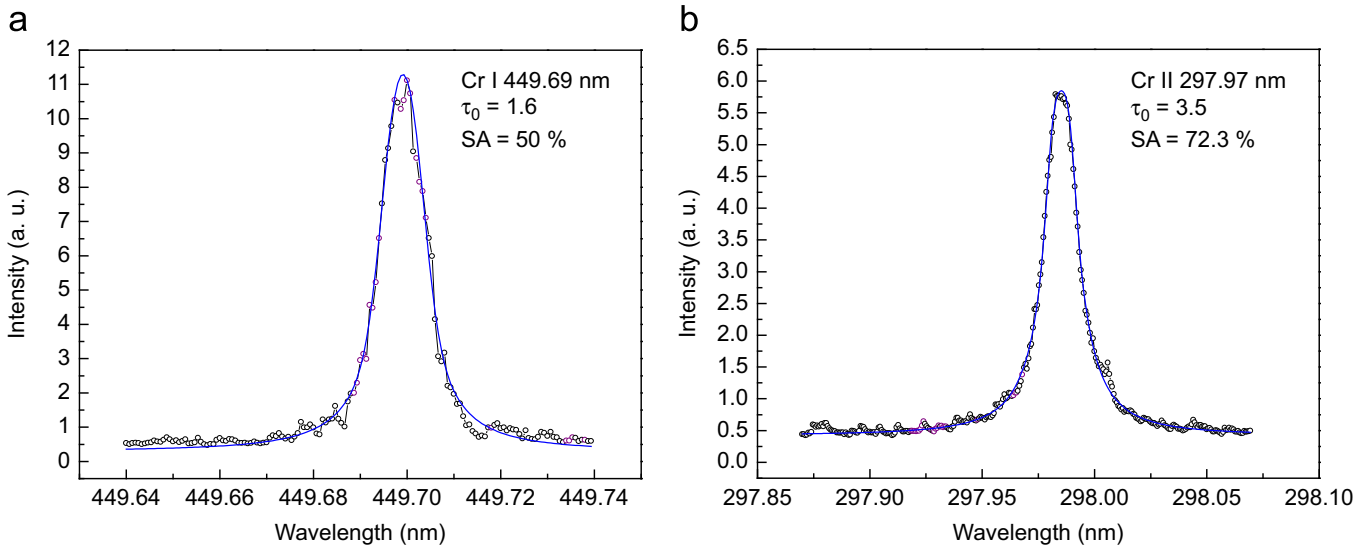

Fig. 2. Examples of experimental profiles (–○–), fitting profiles (–) and line parameters calculated for the lines (a) 449.69 nm Cr I and (b) 297.97 nm Cr II. The maximum optical thicknesses τ_0 and the self-absorption coefficients *SA* are shown.

optically thin conditions (I_{thin}), the value of the optical thickness at the line center (τ_0), the self-absorption coefficient (*SA*), the Stark width (w_{Stark}), and the *A* parameter (Eq. (6)). It can be seen that the analyzed lines were different as a result of their different spectroscopic features. These optical thicknesses originated different degrees of self-absorption that were quantified by the *SA* coefficients. The results of Table 2 were used for characterizing the plasma, as shown in the following section.

4.2. Plasma characterization, homogeneity and self-absorption

The plasma was characterized through the determination of the temperature, electron number density, and *Nl* parameter assuming LTE conditions. The latter is generally fulfilled in LIBS experiments by the relatively high electron densities achieved in the LIP ($\sim 10^{17}$ cm^{-3}). The temperature was determined using the Boltzmann plot method with the optically thin intensities of Cr I–II lines of Table 2.

Fig. 3a and b shows the Boltzmann plots constructed for Cr I and Cr II, respectively. Those lines suffering a low self-absorption (i.e. $SA \leq 35\%$) did not affect significantly the slope of the Boltzmann plots. On the other hand, a proper correction was required for lines appreciably self-absorbed (i.e. $SA > 35\%$). It is observed that the slopes of the linear fittings are different on each case, resulting in different excitation temperatures: $kT_{\mathrm{I}} = (0.62 \pm 0.01)$ eV for Cr I, and $kT_{\mathrm{II}} = (1.22 \pm 0.08)$ eV for Cr II. The errors were derived from the standard deviations of the slopes of the respective linear fittings. This observation agrees with that reported by Aguilera et al. in Ref. [40] describing that different excitation temperatures (called apparent temperatures) are usually obtained for atoms and ions when spatially-integrated line intensities are measured from a LIP. These apparent values are due to population-averaging over the real spatial distribution of species along the line of observation. This result can be extended to all plasma parameters, i.e. the calculated electron and species densities correspond to population-averaged apparent values.

Moreover, in [40], a Saha–Boltzmann plot was constructed with the spatially-integrated emission lines of both ions and neutral atoms. The data were fitted to a straight line giving a unique temperature value between the excitation temperatures for ions and neutral atoms that may be considered as an apparent ionization temperature of the whole plasma. Nevertheless, the authors questioned the reasonability of this value and stressed that it has a considerable dependence on the lines included in the plot.

The Saha–Boltzmann plot is based in the assumption of a homogeneous plasma. Thus, the homogeneity of the LIP was experimentally assessed by comparing the apparent excitation temperatures obtained for ions and neutral atoms. For a homogeneous plasma, both temperature values (and also for the other parameters) should merge into a single value within the experimental error. By contrast, if a relatively large gap between neutral and ionic temperatures is observed, then the plasma inhomogeneity is important, and vice versa. The temperature difference obtained in this work (0.7 eV) provided experimental evidence that the plasma generated in the present experimental conditions had a significative inhomogeneity regarding the Cr concentration, which prevented the construction of the Saha–Boltzmann plot.

In typical LIBS experiences, Stark broadening is the predominant mechanism that determines the Lorentzian contribution to line profiles [41]. It is proportional to the electron number density, namely, $w_{Stark} = 2wN_e/N_e^{Ref}$, where *w* (nm) is the electron impact (half) width, N_e (cm^{-3}) is the electron density, and N_e^{Ref} (cm^{-3}) is a reference electron density, usually 10^{16} or 10^{17} cm^{-3} [4]. Thus, the electron number density is generally determined using the experimentally measured Stark widths from the measured lines. In order to achieve an accurate estimation of the electron density in the core and the periphery regions, an statistical averaging of the results obtained from several lines of Cr I and Cr II should be carried out.

Nevertheless, due to the very scarce published reference Stark coefficients for Cr I–II lines in the pertinent literature (with the only exception of Cr II line at 312.04 nm in

Table 2
Calculated spectroscopic parameters for Cr I–II lines: Experimental intensities (I_{tot}), optically thin intensities (I_{thin}), maximum optical thicknesses (τ_0), self-absorption coefficients expressed as a percentage (SA), Stark widths (w_{Stark}), κ_e factors (Eq. (3)), and A values (Eq. (6)).

Species	Wavelength (nm)	I_{tot} (a. u.)	I_{thin} (a. u.)	τ_0 (adim)	SA (%)	w_{Stark} (Å)	κ_e ($\times 10^{-30}$ m^3)	A ($\times 10^{-10}$ m)
Cr I	380.48	0.624	0.802	1.0	36.7	0.10	0.76	0.121
Cr I	391.92	0.783	1.475	2.9	67.3	0.07	2.77	0.272
Cr I	392.10	0.472	0.543	0.5	21.3	0.08	0.63	0.051
Cr I	392.86	0.301	0.382	0.9	34.0	0.09	0.91	0.099
Cr I	394.15	0.362	0.436	0.7	28.1	0.09	0.67	0.078
Cr I	396.37	1.340	2.492	2.9	67.4	0.08	5.92	0.458
Cr I	396.97	1.164	2.258	3.1	69.2	0.08	4.75	0.387
Cr I	398.39	1.043	1.998	3.0	68.3	0.07	2.92	0.281
Cr I	399.11	0.732	0.989	1.2	41.6	0.09	2.33	0.181
Cr I	403.91	0.294	0.381	1.0	36.8	0.08	0.40	0.102
Cr I	406.57	0.149	0.153	0.1	4.8	0.06	0.10	0.009
Cr I	412.65	0.351	0.391	0.4	17.6	0.09	0.31	0.045
Cr I	420.45	0.163	0.167	0.1	4.8	0.07	0.13	0.009
Cr I	426.31	0.627	0.839	1.1	39.2	0.07	0.53	0.103
Cr I	429.77	0.381	0.460	0.7	28.1	0.08	0.32	0.071
Cr I	430.05	0.190	0.195	0.1	4.8	0.10	0.13	0.012
Cr I	433.76	1.257	1.970	1.9	55.2	0.08	1.48	0.195
Cr I	433.94	1.445	1.903	1.1	39.3	0.10	1.10	0.132
Cr I	434.45	1.950	4.761	5.0	80.1	0.08	5.07	0.508
Cr I	435.10	0.846	1.100	1.0	36.7	0.08	0.68	0.102
Cr I	435.18	2.790	6.534	5.0	80.0	0.10	6.52	0.604
Cr I	435.96	1.634	2.514	1.9	55.2	0.10	1.45	0.230
Cr I	437.13	1.037	1.655	2.0	56.7	0.08	1.50	0.205
Cr I	449.69	1.666	2.442	1.6	50.0	0.09	1.49	0.178
Cr II	284.32	0.918	2.384	6.9	85.5	0.11	3.99	0.775
Cr II	285.68	0.275	0.364	1.2	41.8	0.11	0.78	0.162
Cr II	285.74	0.229	0.304	1.2	41.7	0.11	0.66	0.161
Cr II	286.09	0.724	1.246	2.6	64.3	0.09	1.83	0.296
Cr II	286.26	1.013	2.036	4.1	75.9	0.12	3.23	0.600
Cr II	286.71	0.288	0.453	1.9	55.1	0.12	3.18	0.454
Cr II	286.76	0.927	1.429	2.1	58.2	0.07	1.47	0.372
Cr II	287.04	0.654	1.211	3.1	69.1	0.15	2.36	0.353
Cr II	287.38	0.442	0.629	1.4	46.1	0.09	0.54	0.162
Cr II	287.84	0.384	0.503	1.1	39.3	0.10	0.38	0.144
Cr II	288.09	0.312	0.463	1.8	53.6	0.11	0.97	0.274
Cr II	289.85	0.961	1.424	1.9	55.2	0.13	1.42	0.321
Cr II	292.18	0.737	1.078	1.8	53.5	0.14	0.92	0.284
Cr II	293.08	0.293	0.387	1.2	41.7	0.13	0.51	0.162
Cr II	293.51	0.891	1.434	2.3	60.9	0.11	1.54	0.310
Cr II	295.34	0.288	0.365	1.0	36.7	0.11	0.43	0.135
Cr II	296.60	0.306	0.370	0.8	31.2	0.11	0.47	0.135
Cr II	297.19	1.368	2.758	3.9	74.8	0.14	3.31	0.485
Cr II	297.97	1.379	2.618	3.5	72.3	0.10	2.60	0.473
Cr II	298.92	1.424	2.348	2.6	64.4	0.11	2.18	0.440
Cr II	311.86	1.620	2.912	3.2	70.0	0.14	2.93	0.504
Cr II	312.04	2.051	3.807	3.5	72.3	0.13	3.84	0.591
Cr II	312.87	1.121	1.817	2.4	62.1	0.14	1.40	0.351
Cr II	313.67	1.440	2.169	2.0	56.7	0.12	1.65	0.339

Ref. [42]), it was not possible to conduct a reliable calculus of the electron density. Furthermore, the inhomogeneity of the plasma prevented the calculus of the electron density by using the Saha–Boltzmann equation [41]. From a previous work [41], the electron density for similar experimental conditions can be estimated about $\sim 10^{17}$ cm^{-3}.

For the determination of the parameters Nl, the A values (Eq. (6)) were plotted against the $\kappa_e(T)$ factors (Eq. (3)), which were calculated with the apparent temperatures for Cr I and Cr II lines in the last column of Table 2. As shown in Fig. 4a, b, a linear trend was observed, in accordance with predictions of Eq. (6). This equation expresses, under the present approach, a proportionality between the A values and the $\kappa_e(T)$ factors for a given plasma temperature. The data were then fitted to straight lines passing through zero and the Nl parameters were obtained from the slopes of the linear fittings: $Nl_{\mathrm{I}} = (9.2 \pm 0.3) \times 10^{24}$ cm^{-2} for Cr I and $Nl_{\mathrm{II}} = (1.8 \pm 0.1) \times 10^{25}$ cm^{-2} for Cr II. The errors calculated from the respective standard deviations were statistically reduced by averaging the results obtained from many lines.

Overall, the observations fit well with a picture of a plasma composed of two regions: a core with a higher temperature and populated mainly by ions, surrounded by a periphery with a lower temperature, populated mainly by neutral atoms [30,43,44]. Each region of the plasma is depicted satisfactorily as a homogeneous piece characterized by its own set of plasma parameters and for which the model of Section 2 can be applied. The values of the plasma parameters inside these regions are averaged values of the real spatial distributions.

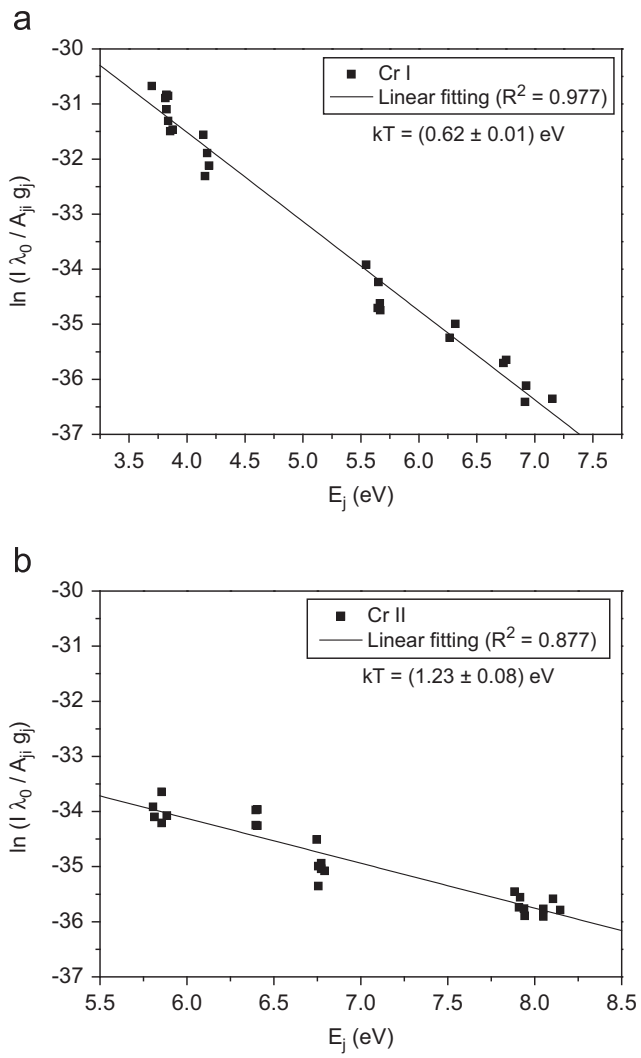

Fig. 3. Boltzmann plots constructed with spatially-integrated optically thin line intensities of Cr I (a) and Cr II (b). Linear fittings and apparent temperatures are shown.

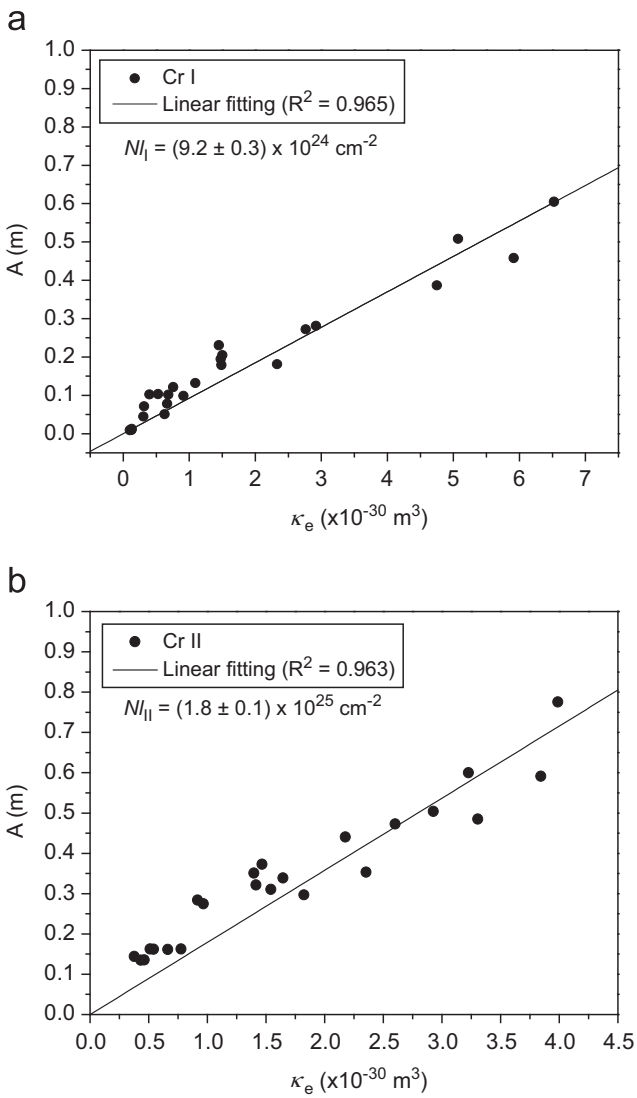

Fig. 4. Plots of A values (Eq. (6)) versus κ_e factors (Eq. (3)) calculated with the apparent temperatures of Cr I and Cr II. Linear fittings and Nl parameters are shown.

The optical thickness of spectral lines, which governs self-absorption, is proportional to the factor $\kappa_e(T)$ (Eq. (2)). Hence, the $\kappa_e(T)$ factors can be calculated for spectral lines through Eq. (3) using a typical range of temperatures to predict their expected self-absorption [36]. Those lines having relatively larger values of κ_e will suffer a stronger self-absorption, and vice versa. For comparison purposes, the SA coefficients obtained experimentally for Cr I–II lines are plotted in Fig. 5a and b with the $\kappa_e(T)$ factors computed with the corresponding apparent temperatures calculated for atoms and ions in Fig. 3a and b, respectively. It was observed that the SA coefficients presented the same trend that the κ_e values for both Cr I and Cr II lines, demonstrating the agreement between model and experiment. In addition, comparing both figures it is seen that Cr II lines are, in general, more self-absorbed than Cr I lines, which can be explained by a larger density of ions respect to neutral atoms.

5. Conclusions

In this paper, the line profiles of several Cr I–II transitions were analyzed line by line for plasma characterization using a simple model of a non-uniform plasma composed of two separate homogeneous regions in LTE: a high-temperature core populated mainly by ions, surrounded by a low-temperature periphery populated mainly by neutral atoms. The emission intensity profiles of Cr I–II lines were measured with good resolution and spatially-integrated along the line of observation. From the individual analysis of the lines, useful information was extracted about spectroscopic data, i.e. total intensity, optical thickness, Stark broadening, and self-absorption. From a joint analysis of the lines, valuable information on plasma properties was deduced, such as atomic and ionic excitation temperatures, spatial inhomogeneity, and Nl parameters for atoms and ions. It was not possible to perform an accurate calculus of the electron density due to the very scarce published reference Stark coefficients for Cr I–II lines. A reliable determination of Stark broadening parameters for Cr lines is envisaged for a future work. Overall, plasma characterization using a simple model provided valuable insight

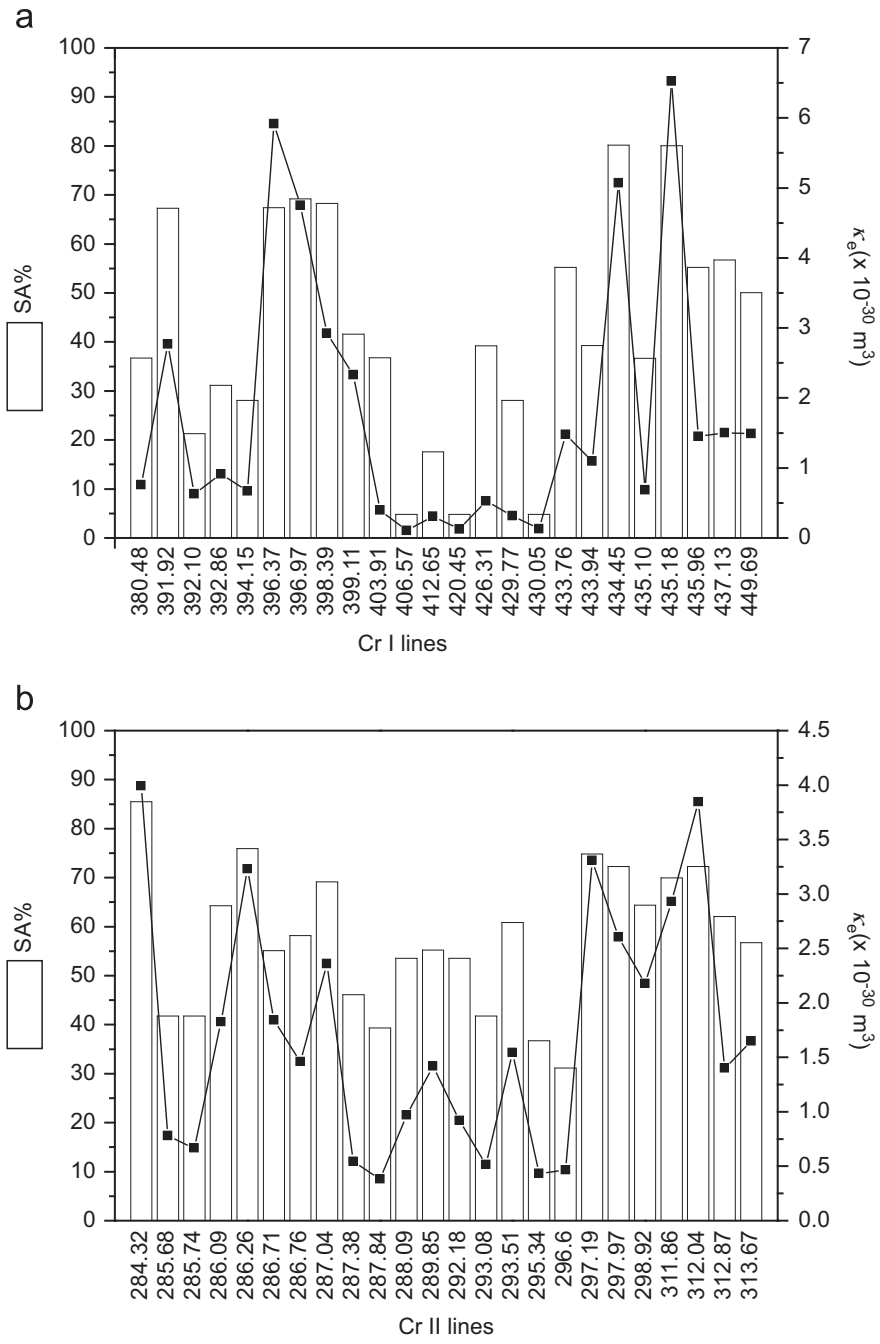

Fig. 5. Comparison of the *SA* coefficients obtained for Cr I (a) and Cr II (b) lines with the κ_e factors of Eq. (3) computed with the corresponding apparent values of temperature obtained from the Boltzmann plots.

about the physical processes involved in LIBS experiments requiring an accurate temperature determination.

Acknowledgments

This work has been supported by the Concejo Nacional de Investigaciones Científicas y Técnicas (CONICET).

References

[1] Miziolek AW, Palleschi V, Schechter I. Laser induced breakdown spectroscopy. Cambridge: Cambridge University Press; 2006.
[2] Cremers DA, Radziemski LJ. Handbook of laser-induced breakdown spectroscopy. Chichester: Wiley; 2006.
[3] Singh JP, Thakur SN. Laser-Induced breakdown spectroscopy. Amsterdam: Elsevier; 2007.
[4] Aragón C, Aguilera JA. Characterization of laser induced plasmas by optical emission spectroscopy: a review of experiments and methods. Spectrochim Acta Part B 2008;63:893–916.
[5] Hahn DW, Omenetto N. Laser-induced breakdown spectroscopy (LIBS), Part I: Review of basic diagnostics and plasma–particle interactions: still-challenging issues within the analytical plasma community. Appl Spec 2010;64:335A–66A.
[6] Tognoni E, Cristoforetti G, Legnaioli S, Palleschi V. Calibration-free laser-induced breakdown spectroscopy: state of the art. Spectrochim Acta Part B 2010;65:1–14.
[7] Aragón C, Bengoechea J, Aguilera JA. Asymmetric Stark broadening of the Fe I 538.34 nm emission line in a laser induced plasma. Spectrochim Acta Part B 2005;60:897–904.

[8] Bengoechea J, Aguilera JA, Aragón C. Application of laser-induced plasma spectroscopy to the measurement of Stark broadening parameters. Spectrochim Acta Part B 2006;61:69–80.
[9] Colón C, Alonso-Medina A. Application of a laser produced plasma: experimental Stark widths of single ionized lead lines. Spectrochim Acta Part B 2006;61:856–63.
[10] Bredice F, Borges FO, Sobral H, Villagran-Muniz M, Di Rocco HO, Cristoforetti G, et al. Measurement of Stark broadening of Mn I and Mn II spectral lines in plasmas used for Laser-Induced Breakdown Spectroscopy. Spectrochim Acta Part B 2007;62:1237–45.
[11] Alonso-Medina A, Colón C, Herrán-Martínez C. Experimentally determined transition probabilities for lines of Pb I and the 2203.5 As line of Pb II. J Quant Spectrosc Radiat Transfer 2001;68:351–62.
[12] Matheron P, Escarguel A, Redon R, Lesage A, Richou J. Si II transition probabilities measurements in a laser induced plasma. J Quant Spectrosc Radiat Transfer 2001;69:535–41.
[13] Alonso-Medina A. A spectroscopic study of laser-induced tin–lead plasma: transition probabilities for spectral lines of Sn I. Spectrochim Acta Part B 2010;65:158–66.
[14] Manrique J, Aguilera JA, Aragón C. Determination of transition probabilities by laser-induced breakdown spectroscopy with curve-of-growth measurements. J Quant Spectrosc Radiat Transfer 2011;112:85–91.
[15] Manrique J, Aguilera JA, Aragón C. Transition probabilities of Ni II spectral lines measured by laser induced breakdown spectroscopy. J Quant Spectrosc Radiat Transfer 2013;120:120–4.
[16] Lochte–Holtgreven W. Evaluation of plasma parameters. In: Lochte-Holtgreven W, editor. Plasma diagnostics. Amsterdam: North-Holland Publishing Company; 1968. p. 214–49.
[17] Griem HR. Principles of Plasma Spectroscopy. Cambridge: Cambridge University Press; 1997.
[18] Tognoni E, Palleschi V, Corsi M, Cristoforetti G. Quantitative micro-analysis by laser-induced breakdown spectroscopy: a review of the experimental approaches. Spectrochim Acta Part B 2002;57:1115–30.
[19] Bulajic D, Corsi M, Cristoforetti G, Legnaioli S, Palleschi V, Salvetti A, et al. A procedure for correcting self-absorption in calibration free-laser induced breakdown spectroscopy. Spectrochim Acta Part B 2002;57:339–53.
[20] El Sherbini AM, El Sherbini ThM, Hegazy H, Cristoforetti G, Legnaioli S, Palleschi V, et al. Evaluation of self-absorption coefficients of aluminum emission lines in laser-induced breakdown spectroscopy measurements. Spectrochim Acta B 2005;60:1573–9.
[21] Bredice F, Borges FO, Sobral H, Villagran-Muniz M, Di Rocco HO, Cristoforetti G, et al. Evaluation of self-absorption of manganese emission lines in Laser Induced Breakdown Spectroscopy measurements. Spectrochim Acta Part B 2006;61:1294–303.
[22] Aguilera JA, Aragón C. Characterization of laser-induced plasmas by emission spectroscopy with curve-of-growth measurements. Part I: Temporal evolution of plasma parameters and self-absorption. Spectrochim Acta Part B 2008;63:784–92.
[23] Moon HY, Herrera KK, Omenetto N, Smith BW, Winefordner JD. On the usefulness of a duplicating mirror to evaluate self-absorption effects in laser induced breakdown spectroscopy. Spectrochim Acta B 2009;64:702–13.
[24] Bredice FO, Di Rocco HO, Sobral HM, Villagrán-Muniz M, Palleschi V. A new method for determination of self-absorption coefficients of emission lines in Laser-induced breakdown spectroscopy experiments. Appl Spec 2010;64:320–3.
[25] Díaz Pace DM, D'Angelo CA, Bertuccelli G. Study of self-absorption of emission magnesium lines in laser-induced plasmas on calcium hydroxide matrix. IEEE Trans Plasma Sci 2012;40:898–908.
[26] Gornushkin IB, Stevenson CL, Smith BW, Omenetto N, Winefordner JD. Modeling an inhomogeneous optically thick laser induced plasma: a simplified theoretical approach. Spectrochim Acta Part B 2001;56:1769–85.
[27] Sakka T, Nakajima T, Ogata YH. Spatial population distribution of laser ablation species determined by self-reversed emission line profile. J Appl Phys 2002;92:2296–303.
[28] Gornushkin IB, Omenetto N, Smith BW, Winefordner JD. Determination of the maximum temperature at the center of an optically thick laser-induced plasma using self-reversed spectral lines. Spectrochim Acta Part B 2004;59:401–18.
[29] Kazakov AY, Gornushkin B, Omenetto N, Smith BW, Winefordner JD. Radiation dynamics of post-breakdown laser induced plasma expanding into ambient gas. Appl Opt 2006;45:2810–20.
[30] D'Angelo CA, Díaz Pace DM, Bertuccelli G, Bertuccelli D. Laser induced breakdown spectroscopy on metallic alloys: solving inhomogeneous optically thick plasmas. Spectrochim Acta Part B 2008;63:367–74.
[31] D'Angelo CA, Díaz Pace DM, Bertuccelli G. Semiempirical model for analysis of inhomogeneous optically thick laser-induced plasmas. Spectrochim Acta Part B 2009;64:999–1008.
[32] Aguilera JA, Aragón C. Characterization of laser-induced plasmas by emission spectroscopy with curve-of-growth measurements. Part I: Temporal evolution of plasma parameters and self-absorption. Spectrochim Acta Part B 2008;63:784–92.
[33] Aguilera JA, Aragón C. Characterization of laser-induced plasmas by emission spectroscopy with curve-of-growth measurements. Part II: Effect of the focusing distance and the pulse energy. Spectrochim Acta Part B 2008;63:793–9.
[34] Thorne A., Litzén U., Johansson S. The width and shape of spectral lines. In: spectrophysics: principles and applications. Berlín: Springer; 1999, p. 187–208.
[35] Zwicker H. Evaluation of plasma parameters in optically thick plasmas. In: Lochte-Holtgreven W, editor. Plasma diagnostics. Amsterdam: North-Holland Publishing Company; 1968. p. 214–48.
[36] Aragón C, Bengoechea J, Aguilera JA. Influence of the optical depth on spectral line emission from laser-induced plasmas. Spectrochim Acta Part B 2001;56:619–28.
[37] Díaz Pace DM, D'Angelo CA, Bertuccelli G. Calculation of optical thicknesses of magnesium emission spectral lines for diagnostics of laser-induced plasmas. Appl Spec 2011;65:1202–12.
[38] Gornushkin IB, Stevenson CL, Smith BW, Omenetto N, Winefordner JD. Modeling an inhomogeneous optically thick laser induced plasma: a simplified theoretical approach. Spectrochim Acta Part B 2001;56:1769–85.
[39] NIST Electronic Database, in ⟨http://physics.nist.gov/PhysRefData⟩.
[40] Aguilera JA, Aragón C. Characterization of a laser-induced plasma by spatially resolved spectroscopy of neutral atom and ion emissions. Comparison of local and spatially integrated measurements. Spectrochim Acta Part B 2004;59:1861–76.
[41] Griem HR. Plasma spectroscopy. New York: McGraw-Hill; 1964.
[42] Konjević N, Wiese WL. Experimental Stark widths and shifts for spectral lines of neutral and ionized atoms (a critical review of selected data for the period 1983 through 1988). J Phys Ref Data 1990;19:1307–85.
[43] Hermann J, Boulmer-Leborgne C, Hong D. Diagnostic of the early phase of an ultraviolet laser induced plasma by spectral line analysis considering self-absorption. J Appl Phys 1998;83:691–6.
[44] Aguilera JA, Bengoechea J, Aragón C. Curves of growth of spectral lines emitted by a laser-induced plasma: influence of the temporal evolution and spatial inhomogeneity of the plasma. Spectrochim Acta Part B 2003;58:221–37.